Dynamic multiple thresholding breast boundary detection algorithm for mammograms

Yi-Ta Wu,[a] Chuan Zhou, Heang-Ping Chan, Chintana Paramagul, Lubomir M. Hadjiiski, and Caroline Plowden Daly
Department of Radiology, University of Michigan, Ann Arbor, Michigan 48109

Julie A. Douglas
Department of Human Genetics, University of Michigan, Ann Arbor, Michigan 48109

Yiheng Zhang, Berkman Sahiner, Jiazheng Shi, and Jun Wei
Department of Radiology, University of Michigan, Ann Arbor, Michigan 48109

(Received 21 January 2009; revised 18 November 2009; accepted for publication 19 November 2009; published 28 December 2009)

Purpose: Automated detection of breast boundary is one of the fundamental steps for computer-aided analysis of mammograms. In this study, the authors developed a new dynamic multiple thresholding based breast boundary (MTBB) detection method for digitized mammograms.
Methods: A large data set of 716 screen-film mammograms (442 CC view and 274 MLO view) obtained from consecutive cases of an Institutional Review Board approved project were used. An experienced breast radiologist manually traced the breast boundary on each digitized image using a graphical interface to provide a reference standard. The initial breast boundary (MTBB-Initial) was obtained by dynamically adapting the threshold to the gray level range in local regions of the breast periphery. The initial breast boundary was then refined by using gradient information from horizontal and vertical Sobel filtering to obtain the final breast boundary (MTBB-Final). The accuracy of the breast boundary detection algorithm was evaluated by comparison with the reference standard using three performance metrics: The Hausdorff distance (HDist), the average minimum Euclidean distance (AMinDist), and the area overlap measure (AOM).
Results: In comparison with the authors' previously developed gradient-based breast boundary (GBB) algorithm, it was found that 68%, 85%, and 94% of images had HDist errors less than 6 pixels (4.8 mm) for GBB, MTBB-Initial, and MTBB-Final, respectively. 89%, 90%, and 96% of images had AMinDist errors less than 1.5 pixels (1.2 mm) for GBB, MTBB-Initial, and MTBB-Final, respectively. 96%, 98%, and 99% of images had AOM values larger than 0.9 for GBB, MTBB-Initial, and MTBB-Final, respectively. The improvement by the MTBB-Final method was statistically significant for all the evaluation measures by the Wilcoxon signed rank test ($p < 0.0001$).
Conclusions: The MTBB approach that combined dynamic multiple thresholding and gradient information provided better performance than the breast boundary detection algorithm that mainly used gradient information.
[DOI: 10.1118/1.3273062]

Key words: breast boundary detection, computer-aided detection, mammogram, multiple thresholding

I. INTRODUCTION

It has been shown that computer-aided detection (CAD) for mammography can increase breast cancer detection sensitivity by radiologists both in the laboratory and in clinical practice.[1–6] Automated detection of breast boundary is one of the fundamental steps for computer-aided analysis of mammograms, including detection of breast lesions,[7,8] estimation of breast density,[9] prediction and correlation of mass location in multiview mammograms,[10–12] and other image analysis applications.[13,14] Breast boundary determination therefore plays an important role in CAD systems.

The breast region of digitized mammograms generally has lower x-ray exposure, and thus higher brightness, than the background outside the breast. However, the breast region cannot be correctly separated from the background by a single threshold value because of the variation in x-ray exposure along the boundary. In addition, the markers and labels in the image background may be connected to the breast if they are placed too close to the breast or if the breast is large. Most breast boundary detection algorithms[9,15–20] share a common approach, in which an initial breast area is obtained by analyzing the gray level histogram and the final breast boundary is determined by a subsequent refinement procedure. These algorithms may fail if the initial breast boundary (MTBB-Initial) deviates too far from the true boundary such that the refinement procedure is misled to the wrong direction.

Bick *et al.*[15] classified the image pixels into potential breast pixels and other background pixels by a modified histogram analysis, and the final breast boundary was derived by region growing and morphological filtering. Ojala *et al.*[17] obtained the initial breast boundary by adaptive histogram thresholding and morphological filtering. The inner stroma edge was extracted by the thresholding method of Otsu,[21] and the next boundary point was predicted by analyzing the Euclidean distance between the inner stroma edge and the outer initial confirmed portion. Three different smoothing procedures, Fourier transform, snake, and *B*-splines, were used to obtain the final breast boundary. Wirth and Stapinski[16] utilized dual thresholding[22] to obtain the initial control points. After performing edge enhancement and noise removal, those control points were input to the snake to obtain the final breast boundary. Ferrari *et al.*[18] determined the initial breast boundary based on the following three steps. First, the image contrast was enhanced using the logarithmic operator. Second, the breast region was thresholded based on the Lloyd–Max quantizer. Third, the binary morphological opening operator was adopted to reduce the noises along the initial breast boundary. In the refinement stage, the final breast boundary was derived by the adaptive active deformable contour model. Sun *et al.*[19] obtained the initial breast boundary by a combination of adaptive thresholding and connected-component analysis, and then determined the initial confirmed portion of the breast boundary by a greedy range selection procedure. They derived the final breast boundary based on the assumption of Euclidean distance constraint between the initial confirmed portion and the stroma edge computed via bimodal histogram analysis. Raba *et al.*[20] determined the initial breast boundary by an adaptive histogram analysis, and then obtained the final boundary by a region growing approach. A fair comparison would require testing the different algorithms with a common data set. Due to the lack of details for some of these published methods, it would be very difficult to implement the methods correctly and compare the accuracy of our and their algorithms in our data set.

We have previously developed a breast boundary detection method by using a gradient-based breast boundary (GBB) technique to search for the breast boundary.[9] The image background was estimated initially by searching for the largest peak in the gray level histogram. After excluding the background from the breast region, an initial edge was derived by a line-by-line gradient analysis from the top to the bottom of the image. The tracking of the breast boundary started from approximately the middle of the breast image and moved upward and downward along the initial boundary. The tracked edges were smoothed to remove noisy fluctuations. In most of these methods, the refinement of the breast boundary may fail if the initial breast boundary was too far from the true boundary.

The initial breast boundary therefore plays an important role in a breast boundary detection system. In this study, we developed a new system for automated breast boundary detection which estimated the initial breast boundary based on a dynamic multiple thresholding method instead of histogram analysis. The final breast boundary was tracked along the initial breast boundary with refinement of the edge location by analysis of the gradient information obtained from horizontal and vertical Sobel filtering. The accuracy of the breast boundary detection was evaluated by comparison with an experienced breast radiologist's manual segmentation. The performance of the new method was also compared to that of our previous method.

II. MATERIALS AND METHODS

II.A. Data sets

A data set of 716 screen-film mammograms (442 CC view and 274 MLO view) were obtained from 288 consecutive cases of an ongoing NIH-supported and Institutional Review Board approved genetic study of breast density in women from the Old Order Amish population of Lancaster County, PA.[23] The mammograms were digitized with a Lumiscan laser scanner at a pixel size of 50×50 μm^2 and 12 bits/pixel. The mammograms were first smoothed with a 16×16 pixel box filter and subsampled by a factor of 16, resulting in a pixel size of 800×800 μm^2 and an approximate image size of 225×300 pixels. For each mammogram, the breast boundary was manually traced by an experienced Mammography Quality Standards Act (MQSA) radiologist. The radiologist used the windowing function to enhance the breast boundary and outlined the breast boundary with the cursor on a graphical user interface. The radiologist's segmented boundaries were used as reference standard for performance evaluation of our method.

II.B. Methods

In order to improve the performance of the breast boundary detection system, we developed a new dynamic thresholding based method, referred to as the multiple thresholding breast boundary (MTBB) detection method. Breast boundary detection is performed in two stages: Initial breast boundary determination and breast boundary refinement. The detailed description for each stage is presented below.

II.B.1. Initial breast boundary determination

As mentioned earlier, the quality of the initial breast boundary is critically important for breast boundary detection. Figure 1 shows an example of obtaining several initial breast boundaries by the thresholding approach using different threshold levels. It is obvious that a single threshold level cannot properly determine the initial breast boundary. For example, in Fig. 1(b), the anterior portion of the initial boundary is closed to the real boundary. However, the boundary encloses a large number of background pixels in the top and bottom areas which will mislead the boundary tracking in the refinement procedure. The relatively high x-ray intensity in these regions is caused by scattered radiation from the chest wall of the patient. Although the background pixels can be removed by selecting a higher threshold level as shown in Figs. 1(c)–1(g), the anterior portion of the initial boundary will then move too far inside the breast as

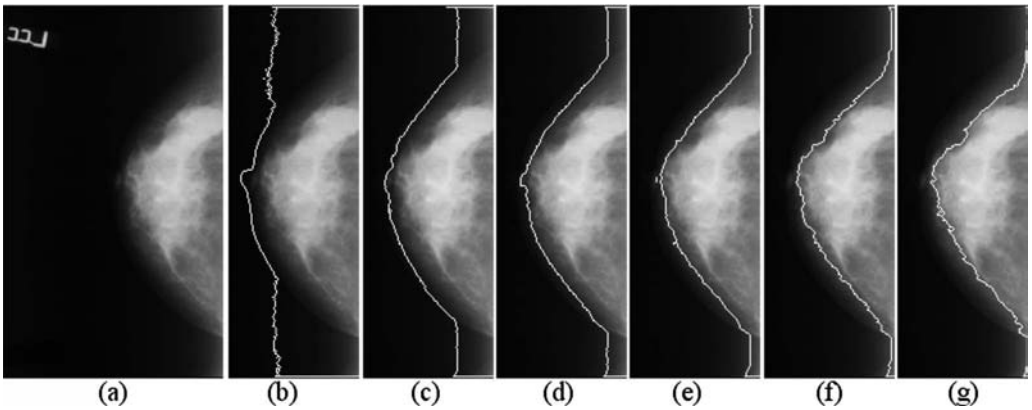

FIG. 1. An example of obtaining several initial breast boundaries by the thresholding approach. (a) The original image with gray levels in range [0,4095]; (b)–(g) the initial breast boundaries derived in threshold levels 300, 500, 700, 900, 1100, and 1300, respectively.

shown in Figs. 1(f) and 1(g). In order to obtain the initial breast boundary as close as possible to the true boundary, we have designed a dynamic multiple thresholding method that contains two steps, breast boundary candidate search, and initial breast boundary extraction, as discussed below.

II.B.1.a. Breast boundary candidate search. Figure 2 shows an example of performing the initial breast boundary candidate (IBBC) search procedure when the breast is on the right side of the mammogram. To initiate the IBBC search, a threshold value h on the image histogram is obtained by the method of Otsu.[21] Let LMX_h be the leftmost x-coordinate of the IBBC at the threshold level h within the middle section of the image (from about 1/4 to 3/4 along the y dimension of the image), as shown in Fig. 2(a). A threshold level l will start from a lower value than h, e.g., $0.5*h$, as shown in Fig. 2(b) and is gradually increased to remove background pixels, guided by a search criterion described below. At a given threshold l, the leftmost x-coordinate LMX_l is determined and a rectangular area having a width of $2*(\text{LM}X\_h-\text{LM}X\_l)$ and centered at LMX_h is defined in the anterior portion of the breast candidate as shown in Fig. 2(c). Note that the width of the rectangular area is decreasing when the threshold l increases, and it will become 0 if the threshold l reaches the high threshold level h obtained by the method of Otsu. Within the rectangle, each column of pixels is searched to determine its intersection with the anterior of the breast region that is above the threshold l. If the pixel column intersects the breast region at more than one contiguous sections, it indicates that the region boundary is not smooth and unlikely to be the breast boundary. The threshold l will then continue to be increased. Figure 2(d) shows that the threshold l search procedure is completed since only a single continuous breast region intersects with each pixel column at the anterior of IBBC. This final threshold l is considered to be the starting threshold level in the boundary tracking procedure below.

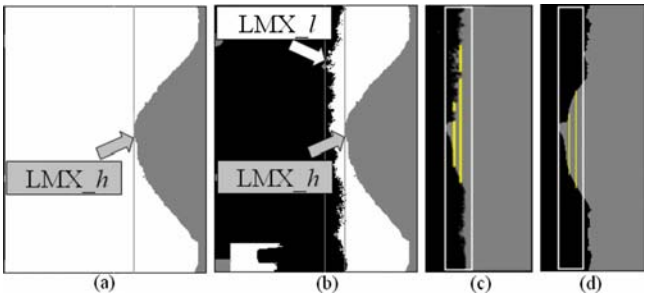

FIG. 2. An example of performing the initial breast boundary candidate search procedure. (a) LMX_h at threshold level h obtained by the Otsu's method. Although the IBBC seems to be close to the true boundary in the anterior portion, it contains many background pixels in the top and bottom chest wall areas. (b) The search of a proper threshold level l for boundary tracking will start from a lower value than h and is gradually increased to remove background pixels. (c) and (d) illustrate the procedure to search for l. The white rectangles in (c) and (d) are centered at the fixed location LMX_h shown in (b), and have a width of $2*(\text{LM}X\_h-\text{LM}X\_l)$ for a given threshold l. The threshold level l is increased after (c) since some columns within the rectangular area contain more than one contiguous section, but stops increasing after (d).

II.B.1.b. Initial breast boundary extraction. Once the IBBC is obtained in the previous step [Fig. 2(d)], the initial breast boundary can be tracked by evaluating the differences between every two thresholded images at consecutive threshold levels as shown in Fig. 3. Figures 3(a) and 3(b) show two thresholded images obtained at two consecutive threshold levels. Figure 3(c) shows the differences (white pixels) between the two thresholded images. The boundary tracking procedure is performed in two parts, the top and bottom portion of the breast boundary that were separated by the white dashed line shown in Fig. 3(d). The location of the line is determined by the vertical coordinate of the leftmost pixel of the IBBC, which may, but not necessarily, be the nipple. For each portion, a new boundary pixel is found in each iteration at the intersection between the central column of the white region and the gray breast region by comparing the two thresholded images. The boundary pixels found in one of the iterations are marked as gray circles in the example shown in Fig. 3(d) (pointed by the white arrow). Figure 4 shows the iterative search of obtaining the MTBB-Initial.

II.B.2. Breast boundary refinement

The refinement procedure of our MTBB detection system tracks the boundary based on the MTBB-Initial and the gra-

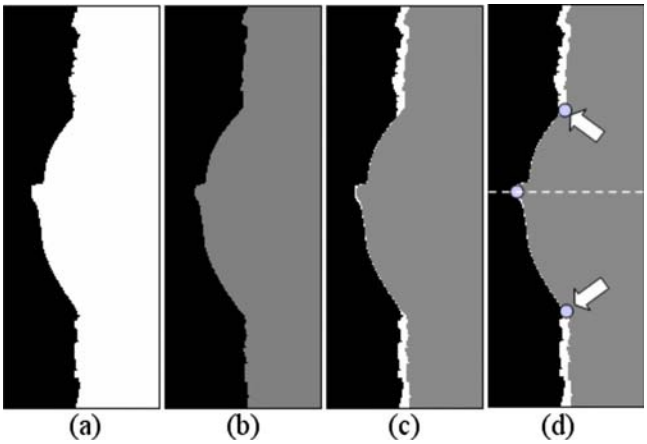

FIG. 3. An example illustrating the breast boundary tracking procedure. (a) and (b) The thresholded images in two consecutive threshold levels. (c) Comparison of the two thresholded images by overlapping. (d) The new breast boundary points are derived by analyzing the differences of the two thresholded images.

dient information. The tracking procedure starts from the same approximately middle point described above [see example in Fig. 3(d)] and moves upward and downward along the initial boundary. The use of the gradient information in the two directions is schematically shown in Fig. 5. The gradient information was obtained by Sobel filtering in the horizontal and vertical directions. The horizontal gradient information (vertical Sobel) is utilized to track the edges in the ranges between A and B and between A and D. The vertical gradient information (horizontal Sobel) is utilized to track the edges in the ranges between B and C and between D and E. The selection of either the vertical or horizontal gradient is determined based on the slope: If the absolute slope of the tangent to the current boundary position is greater than 1, the horizontal gradient is selected; otherwise, the vertical gradient is selected. An example of a mammogram in Fig. 6(a) after vertical and horizontal Sobel filtering is shown in Figs. 6(b) and 6(c), respectively.

The gradient information is one of the references in the refinement procedure; therefore, the tracking procedure will be affected if the gradient information of the breast boundary is distorted by that of artifacts along the boundary area. In order to alleviate this problem, in each step of boundary tracking, three predicted points (A_i, $i=2,3,4$) based on the gradient information and four derived points (B_j, $j=1,2,3,4$) based on the initial breast boundary are estimated as candidates for the next boundary point. Figure 7 shows an example of obtaining the seven points for searching the next boundary point after a boundary point $p(x,y)$ is tracked. The two-step strategy for determining the seven points depends on the region where the breast boundary is being tracked. In the regions using the horizontal gradient information (AB and AD in Fig. 5), the y-coordinates for the seven pixels are first calculated by setting a constant pixel spacing d between each pair of the predicted boundary points and between each pair of the four derived points along the initial breast boundary, i.e., the distances between the y-coordinates of the point pairs (p,A_2), (p,A_3), and (p,A_4) are set to be d, $2d$, and $3d$, respectively, and those between (B_1,B_2), (B_1,B_3), and (B_1,B_4) to be d, $2d$, $3d$, respectively. The y-coordinate of B_1 is the same as that of $p(x,y)$. The points are spaced upward for the upper portion of the breast boundary (AB in Fig. 5) and spaced downward for the lower portion (AD in Fig. 5) from the last tracked point. The x-coordinates of the three predicted boundary points are determined by using the properties of the local horizontal gradient information that the gradient at the boundary is usually high and will gradually decrease as the distance from the boundary increases. The x-coordinates of the four derived points are taken to be the x-coordinates of the initial boundary points at the corresponding y-coordinates. As the boundary tracking proceeds to the regions using the vertical gradient information (BC and DE in Fig. 5), the roles of the x-coordinates and the y-coordinates described above are reversed.

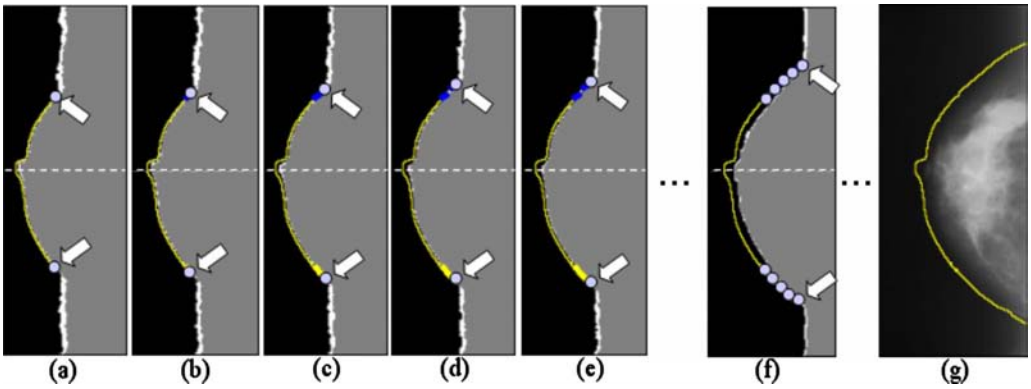

FIG. 4. An example of tracking the initial breast boundary by dynamic multiple thresholding. (a)–(f) show the iterative tracking of the breast boundary in which the white pixels mark the differences between the two consecutive thresholded images, and the light gray circles (pointed out by the arrows) are the boundary points obtained in each iteration of increasing the threshold. (g) The initial breast boundary, MTBB-Initial, is obtained by collecting all the boundary points.

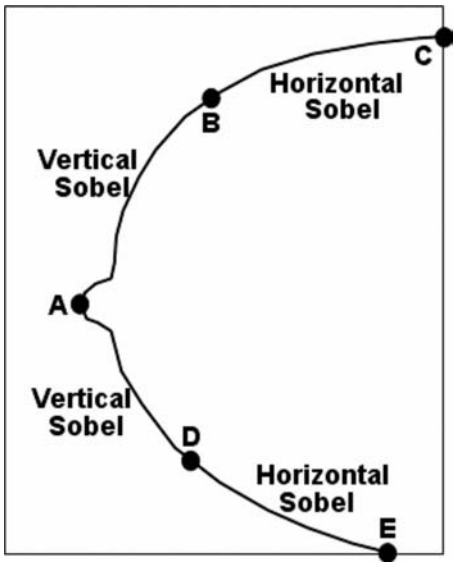

FIG. 5. Vertical and horizontal Sobel filtering used in the breast boundary refinement.

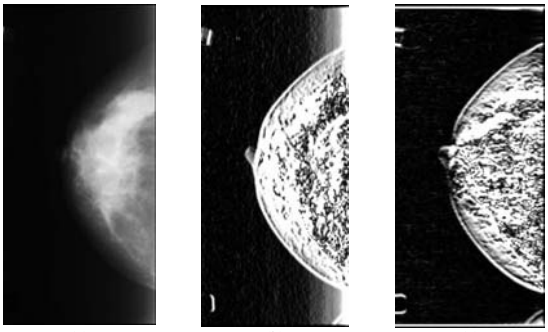

FIG. 6. An example showing (a) an original mammogram, (b) horizontal, and (c) vertical Sobel gradient information.

Once the seven subsequent pixels are derived after a tracked boundary point $p(x,y)$, two types of slopes will be determined to predict the next boundary point as follows.

Type I Slope: Obtained from the tracked boundary point $p(x,y)$ and three predicted points, i.e., the slopes (angles) between lines $\overline{pA_2}$, $\overline{pA_3}$, and $\overline{pA_4}$ and the horizontal line in Fig. 7(b). For example, slope=1 indicates 45° and slope=0 indicates 0°.

Type II Slope: Obtained from the four pixels on the initial breast boundary, i.e., the slopes (angles) between lines $\overline{B_1B_2}$, $\overline{B_1B_3}$, and $\overline{B_1B_4}$ and the horizontal line in Fig. 7(c).

The slope between the current tracked boundary point $p(x,y)$ and its previous tracked points, referred to as the "previous slope," is used as a reference to determine the next boundary point. First, the Type I slopes using the three predicted points A_i $(i=2,3,4)$ are compared to the previous slope. Since the three predicted points are determined based on the gradient information, it is possible that unreasonable predicted points such as markers near the breast boundary are chosen. Let Th_S be the slope change threshold. If at least one of the three differences between the Type I slopes and the previous slope is smaller than or equal to Th_S, the suitable slope will be determined from Type I slopes according to the minimum difference. Otherwise, if the differences between all three Type I slopes and the previous slope are greater than Th_S the abrupt change in slope may indicate the presence of artifacts and we will search for the next boundary point using the Type II slopes. The suitable slope will be considered to be one of the Type II slopes that has the minimum difference from the previous slope. Finally, the coordinate of the next breast boundary point is determined by choosing a constant distance from the current tracked boundary point in the y-coordinate and to calculate the x-coordinate using the "suitable slope" for the regions AB and AD, or correspondingly choosing a constant distance from the x-coordinate followed by calculating the y-coordinate for the regions BC and DE. The constant distances are chosen to be d, $2d$, and $3d$ when selecting the slopes derived from $\overline{B_1B_2}$, $\overline{B_1B_3}$, and $\overline{B_1B_4}$, respectively, which are the same distances as those for setting up the predicted or derived points. If the minimum difference between the Type II slopes and the previous slope is greater than Th_S, a slope change in Th_S is used to determine the next boundary point to avoid sharp direction change in the breast boundary.

The constant pixel spacing d and the slope change threshold Th_S were determined experimentally. The ranges of these parameters were initially estimated by taking into consideration some *a priori* knowledge of breast boundaries. First, since the slope is changing gradually along the breast boundary, the value of the constant pixel spacing should be large enough to avoid an abrupt slope change. For example, if the pixel spacing is too small, e.g., 1 pixel, the tracking procedure will be sensitive to noise. The slopes will have large fluctuations and the determination of the next boundary point by comparing the slope differences will be unreliable. Second, since the breast boundary is smooth, the value of the constant pixel spacing should be small enough to provide adequate sampling of the boundary curve. For example, if the pixel spacing is set to be too large, e.g., 30 pixels, two problems may arise: One is that the slope along the breast boundary may change by a large amount and the use of the previous slope as a guide may not be meaningful, and the other is that the final breast boundary points will be piecewise linear. Our experiments indicated that a spacing of 3–5 pixels is the best range to perform the refinement procedure when images with 800 μm pixel size are used. In this study, we chose $d=3$ pixels. Similarly, for the slope change threshold Th_S, if it is too small, e.g., 1°, the tracking procedure prefers to find a nearly straight line along the breast boundary, but the true boundary is curved gradually. On the other hand, if the slope threshold is set to be too large, e.g., 45°, the tracking procedure will allow an abrupt angle change and thus may not be able to avoid a marker or label that overlaps with the breast boundary. Our experiments indicate that 10°–20° is the best range, and we chose $\mathrm{Th}_S=0.3$ (around 17°) in this study.

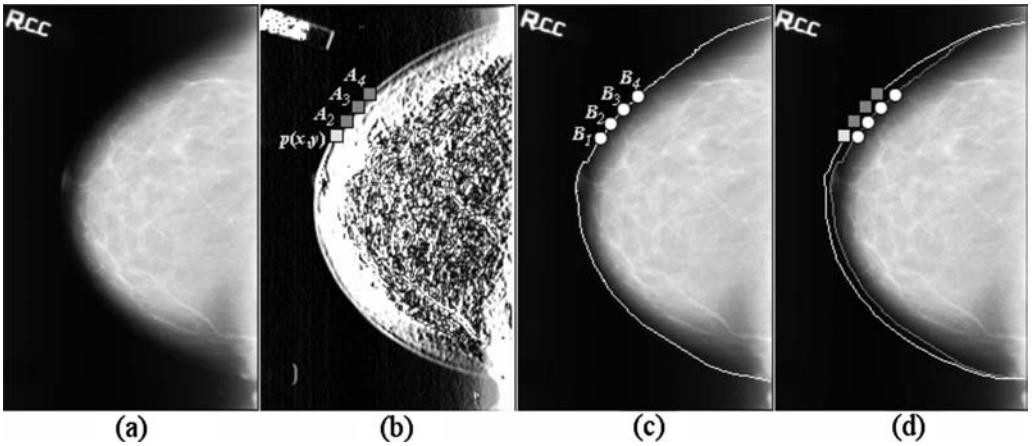

FIG. 7. An example of obtaining the seven subsequent points following the determination of a given tracked boundary point $p(x,y)$. (a) Original mammogram; (b) vertical Sobel filtered image showing the three predicted boundary points (dark gray squares), which fall on the final breast boundary in most cases; (c) original mammogram superimposed with the initial breast boundary and the four derived points (white circles); and (d) demonstration of the seven points along the initial (white) and final (gray) breast boundaries.

II.B.3. Evaluation methods

Two distance measures and one similarity measure are used to compare the automatically detected breast boundary $T=\{t_1,t_2,\cdots,t_p\}$, which contains p points with the experienced radiologist's manually traced boundary $R=\{r_1,r_2,\cdots,r_q\}$, which contains q points. More detailed descriptions regarding those measures can be found in our previous study.[24] The minimum Euclidean distance $\mathrm{MinDist}(\alpha,R)$ between a point α and a curve $R=\{r_1,r_2,\cdots,r_q\}$ is defined as

$$\mathrm{MinDist}(\alpha,R)=\min_{i\in\{1,2,\cdots,q\}}\|\alpha-r_i\|. \tag{1}$$

The Hausdorff distance (HDist) (Ref. 25) $\mathrm{HDist}(T,R)$ is used to evaluate the maximum distance between the two curves, and it is defined in terms of the directed Hausdorff distance as

$$\mathrm{HDist}(T,R)=\max\{h\mathrm{Dist}(T,R),h\mathrm{Dist}(R,T)\} \tag{2}$$

in which the directed Hausdorff distance $h\mathrm{Dist}(T,R)$ identifies the maximum among the distances from the points along curve T to curve R,

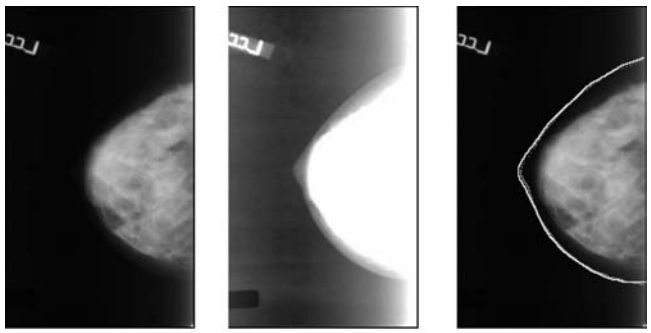

FIG. 8. (a) Original mammogram. (b) The windowed image of (a) to emphasize the breast boundary. (c) The initial (inner gray line) and the final (outer white line) breast boundaries.

$$h\mathrm{Dist}(T,R)=\max_{i\in\{1,2,\cdots,p\}}\{\mathrm{MinDist}(t_i,R)\}. \tag{3}$$

Another distance measure, referred to as the average minimum distance $\mathrm{AMinDist}(T,R)$ is used to evaluate how much curves T and R are dissimilar on average. $\mathrm{AMinDist}(T,R)$ is defined by averaging the MinDist of T to R and the MinDist of R to T

$$\mathrm{AMinDist}(T,R)=\frac{\sum_{i=1}^{p}\mathrm{MinDist}(t_i,R)}{2p}+\frac{\sum_{i=1}^{q}\mathrm{MinDist}(r_i,T)}{2q}. \tag{4}$$

The distance measures were calculated in units of pixels (1 pixel=0.8 mm) in this study.

The similarity measure used in this study is the area overlap measure (AOM) between two curves enclosing the breast region, which are formed by T or R at the breast boundary, the chest wall, and the image boundary at the top of the pectoral muscle for MLO view, defined as

$$\mathrm{AOM}(T,R)=\frac{\mathrm{Area}\{S_T\cap S_R\}}{\mathrm{Area}\{S_T\cup S_R\}}, \tag{5}$$

where S_T and S_R are the interior regions enclosed by the two closed curves, respectively.

III. RESULTS

III.A. Breast boundary detection examples

Figures 8–10 show examples of the initial and the final breast boundary detection results using our MTBB system. Figure 8 shows an example in which the initial breast boundary is very close to the final boundary. Figure 9 shows an example that has a high intensity marker near the top-left breast area. This is a difficult case since the edge gradient will lead the refinement procedure to the wrong direction. However, by using the initial breast boundary as a guide, the

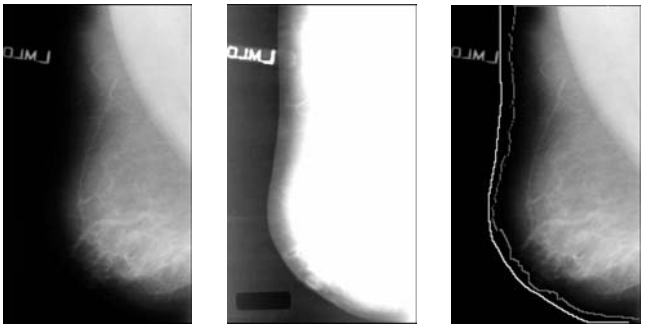

(a) (b) (c)

FIG. 9. (a) Original mammogram containing a high intensity marker (the LMLO label) near the top-left boundary. (b) The windowed image of (a) to show the breast boundary. (c) The initial (inner gray line) and the final (outer white line) breast boundaries.

final breast boundary tracked by the MTBB algorithm is close to the true boundary. Figure 10 shows another example containing a low intensity label covering a small section of the anterior breast boundary. Again, the final breast boundary is closer to the true boundary than the initial boundary.

III.B. Performance evaluation

We evaluated the performance of our dynamic MTBB detection method in comparison with the radiologist's manual segmentation. We also compared the performance of MTBB to our previously developed GBB detection approach.[9] Table I and Fig. 11 show the MTBB method achieved smaller distance errors and slightly larger AOMs than the GBB method. The *P*-values of two-tailed Wilcoxon signed rank test on the following three comparisons (GBB vs MTBB-Initial), [GBB vs final breast boundary (MTBB-Final)], and (MTBB-Initial vs MTBB-Final) using the three evaluation measures are shown in Table II. All comparisons show that the improvement achieved with our newly developed method (MTBB-Final) is statistically significant.

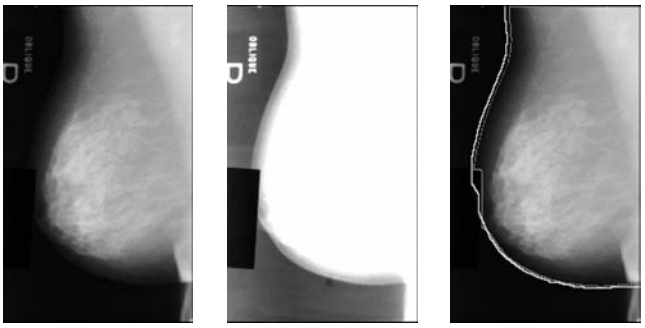

(a) (b) (c)

FIG. 10. (a) Original mammogram containing a low intensity object (the shadow of a label) covering a small section of the left breast boundary. (b) The windowed image of (a) to show the breast boundary. (c) The initial (inner gray line) and the final (outer white line) breast boundaries.

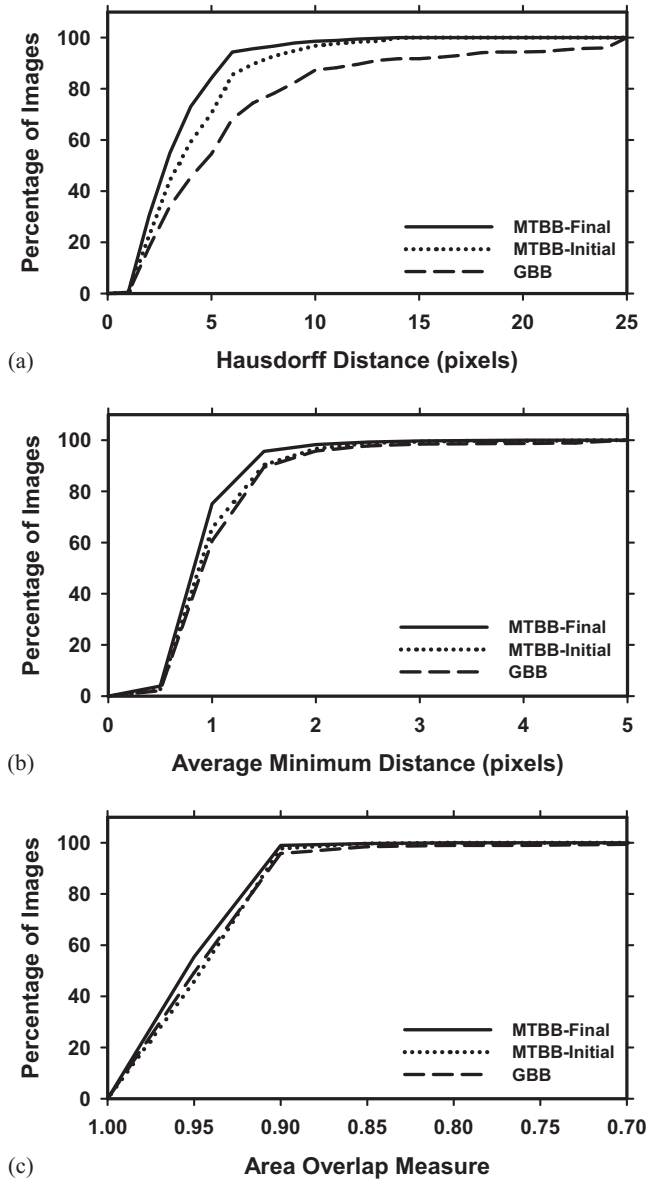

FIG. 11. Cumulative counts of the number of images having the performance measure; (a) Hausdorff distance and (b) average minimum Euclidean distance, less than a given value, and (c) area overlap greater than a given value by comparing the automated breast boundary detection to an MQSA radiologist's manual segmentation.

IV. DISCUSSION

The initial breast boundary plays an important role in the breast boundary detection system since it can lead the tracking or refinement procedure to avoid artifacts along the breast boundary. Figure 12 shows an example in which a label is in contact with the nipple region. Figure 12(a) shows that the GBB was diverted to the edge of the label (gray line), while the new MTBB method successfully tracked the boundary (white line). In this example, the dynamic multiple thresholding method correctly identified the initial breast boundary but the GBB method initially found the edge of the label because of the simple line-by-line search. The subsequent refinement could not correct for this major error because it deviated too far from the true boundary. For the

TABLE I. Comparison of automated boundary detection with an experienced radiologist's manual segmentation for 716 mammograms.

	GBB (%)	MTBB-Initial (%)	MTBB-Final (%)
Percentage of images having HDist error less than 6 pixels (4.8 mm)	68	85	94
Percentage of images having AMinDist error less than 1.5 pixels (1.2 mm)	89	90	96
Percentage of images having AOM values larger than 0.9	96	98	99

cases without markers or labels along the boundary, the initial breast boundary still serves as an important guide for the tracking procedure, especially in regions where the boundary is closed to the nipple or chest wall. Figure 13 shows an example comparing the GBB method (gray line) and MTBB-Final (white line) results. In order to extract the nipple, the GBB method used a lax criterion to search for the edge while tracking the boundary. However, the lax criterion is sensitive to noise and thus GBB found an outer edge, probably due to scattered radiation, around the nipple region. The strong scattered radiation near the chest wall caused a similar problem. In these situations, the combined information from the Sobel gradients and the initial breast boundary used in the refinement stage of the MTBB method guided the tracking to the correct boundary. These examples demonstrated that the MTBB method can improve the nipple location and shape along the breast boundary. This will likely improve the accuracy of automated nipple detection for multiple view analysis.

Our experiences in breast boundary detection indicate that the initial breast boundary has a strong impact on the overall accuracy of breast boundary detection. The complexity of the refinement procedure will likely depend on the difference between the initial breast boundary and the true boundary, i.e., the farther the initial breast boundary is from the true

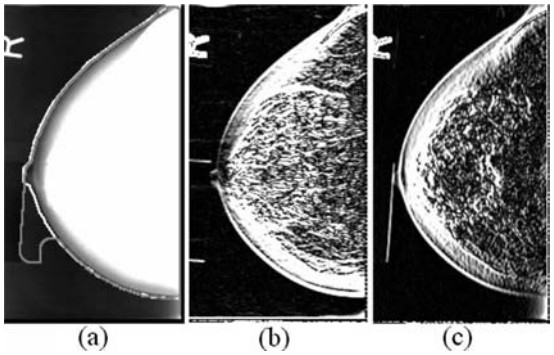

FIG. 12. An example, in which a label is connected to the nipple region, showing (a) the GBB (gray line) and MTBB-Final (white line) results, (b) vertical, and (c) horizontal gradient information by Sobel filtering. In comparison to manual segmentation, the AOM, HDist, and AMinDist measures for the GBB boundary were 0.929 and 20.22 pixels, and 1.52 pixels, respectively, and those for the MTBB-Final boundary were 0.976 and 2.45 pixels, and 0.32 pixels, respectively.

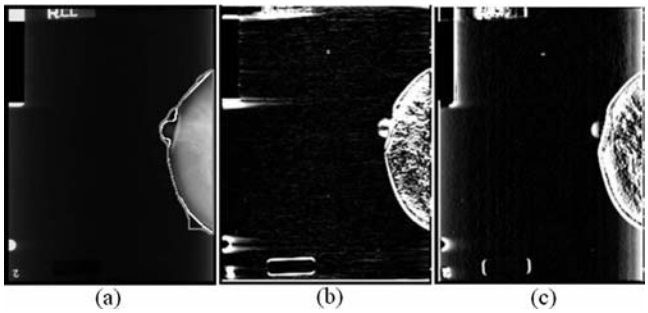

FIG. 13. An example showing (a) the GBB (gray line) and MTBB-Final (white line) results, (b) vertical, and (c) horizontal gradient information by Sobel filtering. In comparison to manual segmentation, the AOM, HDist, and AMinDist measures for the GBB boundary were 0.893 and 8.54 pixels, and 1.34 pixels, respectively, and those for the MTBB-Final boundary were 0.969 and 2.24 pixels, and 0.43 pixels, respectively.

one, the more complicated techniques and rules may be needed during the refinement process to find the optimal boundary. Many breast boundary detection systems obtain the initial breast boundary by thresholding. However, our study indicated that it is difficult to obtain a reasonable initial boundary by using a simple thresholding approach. In this study, we developed a dynamic multiple thresholding approach to obtain the initial breast boundary. The key steps of our method include (1) the initial accurate determination of the anterior region of the breast region; (2) the gradual increase in the threshold from low to high levels starting from the breast anterior region; (3) limiting the search for initial boundary points only within a small breast peripheral region at each level; and (4) analyzing the differences between two thresholded images at consecutive threshold levels to prevent large change in the boundary direction. The adaptation of the thresholding to the local breast boundary improves the chance that the initial breast boundary is close to the true boundary despite the variation in the x-ray intensity in the breast boundary region. Furthermore, in the refinement process, the search for the next boundary point is guided by the previously tracked breast boundary direction and the comparison of multiple boundary point candidates. Both techniques reduce the chance of tracking into artifacts at the breast boundary. Because only a small fraction of the mammograms will have the problem of artifacts or noise at the breast boundary, the overall improvement in the performance measures over the entire data set by our new breast boundary tracking methods only changed by small fractions. However, this small fraction of problematic cases, for which commonly used boundary detection methods would fail, makes it diffi-

TABLE II. The two-tailed *P*-values of the improvement in the breast boundary accuracy estimated from Wilcoxon signed rank test between pairs of the three methods.

	HDist	AMinDist	AOM
GBB vs MTBB-Initial	<0.0001	<0.0001	0.50
GBB vs MTBB-Final	<0.0001	<0.0001	0.0006
MTBB-Initial vs MTBB-Final	<0.0001	0.0002	<0.0001

cult to fully automate the image analysis process in many CAD systems such as nipple detection, multiview correlation of lesion detection or characterization.[12,26–30] The improvement achieved by the new method is a step toward full automation of these processes.

The AOM is a commonly used metric for comparison of the agreement between two segmented objects. However, it is well known that AOM does not clearly reveal spurious errors that do not cause a large difference in the segmented object area. For the breast boundary detection problem, one major source of error is the artifacts that cause local deviations in the boundary as demonstrated in the examples in Figs. 10, 12, and 13. We therefore chose the Hausdorff distance to measure this type of errors. The average minimum Euclidian distance (AMinDist) is a commonly used measure of the average distance between two curves that can more specifically than the AOM show the deviation between the boundaries. In addition, the AMinDist provides the average rather than the maximum of the differences and is thus complementary to the Hausdorff distance.

To estimate the intraobserver and interobserver variabilities in the manual segmentation, a subset of 50 CC view and 50 MLO view mammograms was randomly selected from the data set of 716 mammograms. The same radiologist (R1) who provided the reference standard for the entire data set and a second MQSA radiologist (R2) were asked to outline the breast boundaries of the subset more than a year after the first segmentation. The radiologists performed the new segmentation independently without knowledge of the previous segmentations. The similarity measure, AOM, and distance measures AMinDist and HDist, between pairs of the segmentations, denoted by R1(1), R1(2), and R2, were calculated The intraobserver variability was estimated by the three measures between R1(1) and R1(2), and the interobserver variability was estimated by the three measures between R1(1) and R2 or between R1(2) and R2, as shown in Fig. 14. The intraobserver variation was slightly smaller than the interobserver variations; however, the differences in either the interobserver or intraobserver variations did not achieve statistical significance for these two experienced radiologists, as estimated by the two-tailed *P*-values of the Wilcoxon signed rank test (Table III). In comparison to the results in Fig. 11, the differences between the current (MTBB) and previous (GBB) methods are much greater than the interobserver and intraobserver variations, especially for the Hausdorff distance that measures the sporadic large deviations from the reference boundary, which was substantially reduced by the MTBB method.

Our algorithms involve several parameters. We determined these parameters empirically by experimenting with small subsets of the available data set. To evaluate the consistency of the algorithm performance in the large data set, we randomly grouped the 716 images by case into two subsets, each with 358 images. We calculated the three performance measures AOM, AMinDist, and HDist, and estimated the significance in their differences between the two subsets using the nonparametric Mann–Whitney test for unpaired data. The two-tailed *P*-values for the three measures were

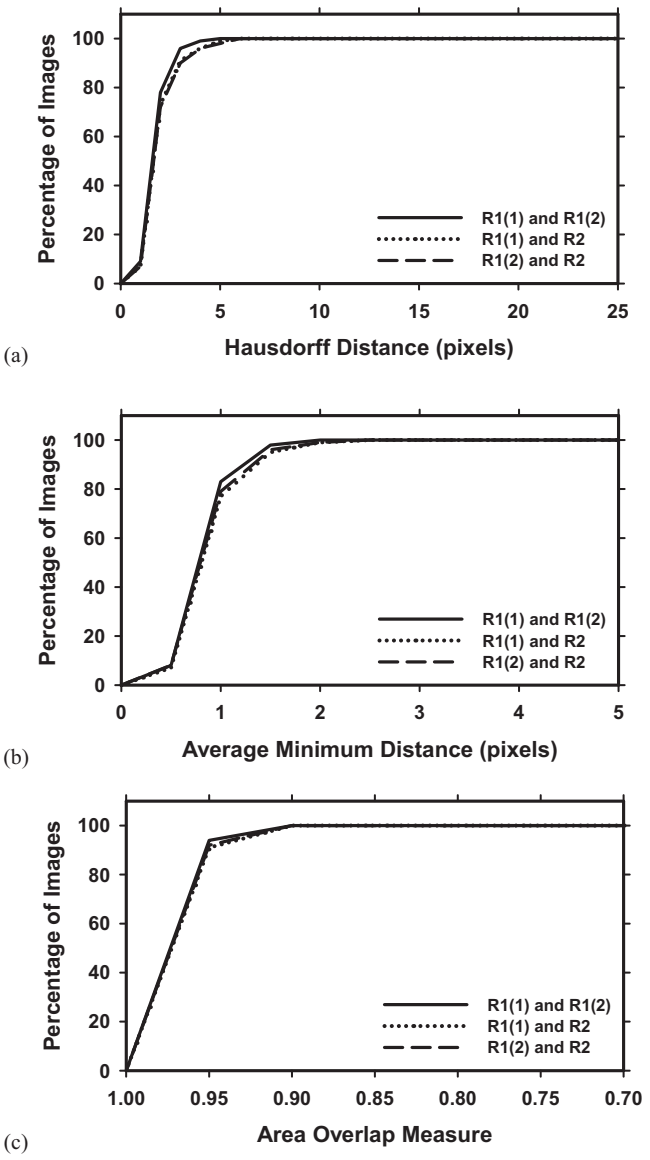

FIG. 14. Cumulative counts of the number of images having the performance measures; (a) Hausdorff distance and (b) average minimum Euclidean distance, less than a given value, and (c) area overlap greater than a given value by comparing the two segmentations R1(1) and R1(2) by the first radiologist, and one segmentation R2 by the second radiologist.

0.19, 0.54, and 0.26, respectively. We repeated the same experiment with two other different groupings. The two-tailed *P*-values were 0.54, 0.07, and 0.15, respectively, for the second grouping and 0.50, 0.42, and 0.61, respectively, for the third grouping. These experiments indicate that there were no significant differences in the performance measures between the random subsets of images. Therefore, although our chosen parameters may not be optimal and the performance was not evaluated in an independent test set, we expect that the parameters used would be reasonably robust because the validation sample size of over 700 used in this study was relatively large. Even if the entire set was used for training, the training performance would approach that of test performance when the training sample size is sufficiently large.[31,32]

The breast boundary detection algorithm developed in this

TABLE III. The two-tailed *P*-values estimated from the Wilcoxon signed rank test on the differences in the breast boundaries between pairs of the R1 and R2 segmentations obtained by the three performance measures. R1(1) = first outline by R1, R1(2) = second outline by R1, R2 = outline by R2. The performance measure was calculated relative to each of the radiologist's segmentations as "reference" shown in column 2.

	Reference	HDist	AMinDist	AOM
R1(2) and R1(1) vs R2 and R1(1)	R1(1)	0.09	0.49	0.19
R1(1) and R1(2) vs R2 and R1(2)	R1(2)	0.10	0.14	0.052
R1(1) and R2 vs R1(2) and R2	R2	0.97	0.36	0.61

study is mainly useful for digitized mammograms. For digital mammograms, the breast laterality and view label is usually shown only on the viewing workstation so that they will not contribute artifacts to breast boundary detection using the digital files. The breast boundaries are also easier to detect, especially in the "for presentation" images. However, screen-film mammography is still commonly used in breast imaging clinics to date and may continue to be a competitive modality in years to come since digital mammography systems are much more expensive and have not been found to be superior to screen-film mammography in all types of breasts.[33] Improvement of the CAD methods for screen-film mammography will continue to be an important area of research. Improving the accuracy of breast boundary detection will be the fundamental step in implementing many advanced techniques that can enhance CAD performance.

Although our MTBB algorithm can circumvent the problem of markers or other artifacts overlapping with the breast boundary in most of the cases as demonstrated in Figs. 9 and 10, there are still two cases in which our algorithm failed to exclude the object when the high intensity object happened to be the leftmost point in the initial breast boundary, as shown in an example in Fig. 15. In such cases, the refinement procedure would take the object as the starting point and then moved upward and downward along the initial boundary. The marker would therefore not be excluded by the proposed method. We believe this problem may be alleviated either by designing more intelligent criteria on the selection of the starting point, or by performing a postprocessing procedure to identify unusual shape regions along the breast boundary and refine the boundary locally. Further work is underway to reduce these errors.

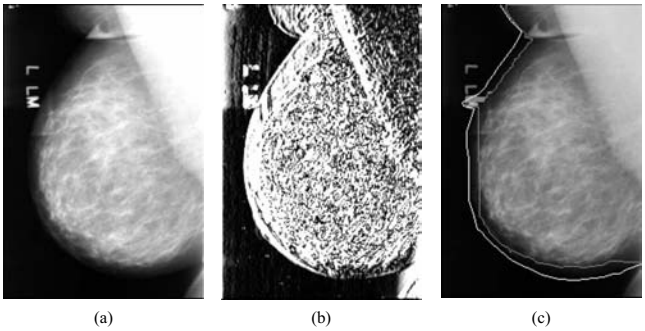

(a) (b) (c)

FIG. 15. (a) Original mammogram containing a high intensity marker. (b) The vertical Sobel filtered image of (a) to show the horizontal gradient information. (c) The initial (inner gray line) and the final (outer white line) breast boundaries. The marker was considered as the starting point for the refinement procedure so that the final result contained the marker.

V. CONCLUSIONS

Many breast boundary detection systems obtain the breast boundary by first determining an initial boundary which is used to guide the tracking of a final boundary. However, those systems may fail due to errors in the initial boundary. Our MTBB system determines the initial boundary based on dynamic adaptation of the threshold to local regions of the breast periphery. The final boundary is then tracked based on the initial boundary and the gradient information. In comparison to a gradient-based method, the new method reduces the chances that the detected breast boundary would be misled by artifacts and noise along the breast boundary. The new method improved the agreement between the automated detected breast boundary and that manually outlined by an experienced breast radiologist, as estimated by three performance measures, the HDist errors, the AMinDist errors, and the area overlap. Our results demonstrate that the analysis of thresholded images based on dynamic adaptation of threshold levels is a robust approach to the detection of breast boundary.

ACKNOWLEDGMENTS

This work is supported by USPHS Grant No. RO1 CA95153. The genetic study of breast density in the Amish population is supported by USPHS Grant No. R01 CA122844 (P.I. Julie Douglas, Ph.D.). The content of this article does not necessarily reflect the position of the funding agencies and no official endorsement of any equipment and product of any companies mentioned should be inferred.

[a]Author to whom correspondence should be addressed. Electronic mail: yitawu@itri.org.tw; Telephone: 734-647-8553; Fax: 734-615-5513.

[1]H. P. Chan, K. Doi, C. J. Vyborny, R. A. Schmidt, C. E. Metz, K. L. Lam, T. Ogura, Y. Wu, and H. MacMahon, "Improvement in radiologists' detection of clustered microcalcifications on mammograms. The potential of computer-aided diagnosis," Invest. Radiol. **25**, 1102–1110 (1990).

[2]L. J. Warren Burhenne, S. A. Wood, C. J. D'Orsi, S. A. Feig, D. B. Kopans, K. F. O'Shaughnessy, E. A. Sickles, L. Tabar, C. J. Vyborny, and R. A. Castellino, "Potential contribution of computer-aided detection to the sensitivity of screening mammography," Radiology **215**, 554–562 (2000).

[3]T. W. Freer and M. J. Ulissey, "Screening mammography with computer-aided detection: Prospective study of 12,860 patients in a community breast center," Radiology **220**, 781–786 (2001).

[4]R. F. Brem, J. K. Baum, M. Lechner, S. Kaplan, S. Souders, L. G. Naul, and J. Hoffmeister, "Improvement in sensitivity of screening mammography with computer-aided detection: A multi-institutional trial," AJR, Am. J. Roentgenol. **181**, 687–693 (2003).

[5]S. V. Destounis, P. DiNitto, W. Logan-Young, E. Bonaccio, M. L. Zuley, and K. M. Willison, "Can computer-aided detection with double reading of screening mammograms help decrease the false-negative rate? Initial experience," Radiology **232**, 578–584 (2004).

[6]M. A. Helvie *et al.*, "Sensitivity of noncommercial computer-aided detection system for mammographic breast cancer detection—A pilot clinical trial," Radiology **231**, 208–214 (2004).

[7]N. Petrick, H. P. Chan, B. Sahiner, and M. A. Helvie, "Combined adaptive enhancement and region-growing segmentation of breast masses on digitized mammograms," Med. Phys. **26**, 1642–1654 (1999).

[8]J. Wei, B. Sahiner, H. P. Chan, N. Petrick, L. M. Hadjiiski, and M. A. Helvie, "Computer aided diagnosis system for mass detection: Comparison of performance on full-field digital mammograms and digitized film mammograms," Radiological Society of North America, Program Book, p. 387 (2003).
[9]C. Zhou, H. P. Chan, N. Petrick, M. A. Helvie, M. M. Goodsitt, B. Sahiner, and L. M. Hadjiiski, "Computerized image analysis: Estimation of breast density on mammograms," Med. Phys. **28**, 1056–1069 (2001).
[10]L. M. Hadjiiski, B. Sahiner, E. M. Caoili, R. H. Cohan, and H. P. Chan, "Automated detection of ureter abnormalities on multidetector row CT urography," Proc. SPIE **6144**, 1W1–1W7 (2006).
[11]B. Sahiner, N. Petrick, H. P. Chan, S. Paquerault, M. A. Helvie, and L. M. Hadjiiski, "Recognition of lesion correspondence on two mammographic views—A new method of false-positive reduction for computerized mass detection," Proc. SPIE **4322**, 649–655 (2001).
[12]S. Paquerault, N. Petrick, H. P. Chan, B. Sahiner, and M. A. Helvie, "Improvement of computerized mass detection on mammograms: Fusion of two-view information," Med. Phys. **29**, 238–247 (2002).
[13]C. Zhou, H.-P. Chan, C. Paramagul, M. A. Roubidoux, B. Sahiner, L. M. Hadjiiski, and N. Petrick, "Computerized nipple identification for multiple image analysis in computer-aided diagnosis," Med. Phys. **31**, 2871–2882 (2004).
[14]Y. Zhang, H.-P. Chan, B. Sahiner, Y.-T. Wu, C. Zhou, J. Ge, J. Wei, and L. M. Hadjiiski, "Application of boundary detection information in breast tomosynthesis reconstruction," Med. Phys. **34**, 3603–3613 (2007).
[15]U. Bick, M. L. Giger, R. A. Schmidt, R. M. Nishikawa, D. E. Wolverton, and K. Doi, "Automated segmentation of digitized mammograms," Acad. Radiol. **2**, 1–9 (1995).
[16]M. A. Wirth and A. Stapinski, "Segmentation of the breast region in mammograms using snakes," in Proceedings of the First Canadian Conference on Computer and Robot Vision, 2004, pp. 385–392 (unpublished).
[17]T. Ojala, J. Nappi, and O. Nevalainen, "Accurate segmentation of the breast region from digitized mammograms," Comput. Med. Imaging Graph. **25**, 47–59 (2001).
[18]R. J. Ferrari, R. M. Rangayyan, J. E. L. Desautels, R. A. Borges, and A. F. Frere, "Identification of the breast boundary in mammograms using active contour models," Med. Biol. Eng. Comput. **42**, 201–208 (2004).
[19]Y. Sun, J. S. Suri, J. E. L. Desautels, and R. M. Rangayyan, "A new approach for breast skin-line estimation in mammograms," Pattern Anal. Appl. **9**, 34–47 (2006).
[20]D. Raba, A. Oliver, J. Marti, M. Peracaula, and J. Espunya, "Breast segmentation with pectoral muscle suppression on digital mammograms," in *Pattern Recognition and Image Analysis*, Lecture Notes in Computer Science Vol. 3523 (Springer, Berlin/Heidelberg, 2005), pp. 471–478.
[21]N. Otsu, "A threshold selection method from gray-level histograms," IEEE Trans. Syst. Man Cybern. **9**, 62–66 (1979).
[22]P. L. Rosin, "Unimodal thresholding," Pattern Recogn. **34**, 2083–2096 (2001).
[23]J. A. Douglas, M.-H. Roy-Gagnon, C. Zhou, B. D. Mitchell, A. R. Shuldiner, H.-P. Chan, and M. A. Helvie, "Mammographic breast density—Evidence for genetic correlations with established breast cancer risk factors," Cancer Epidemiol. Biomarkers Prev. **17**, 3509–3516 (2008).
[24]B. Sahiner, N. Petrick, H. P. Chan, L. M. Hadjiiski, C. Paramagul, M. A. Helvie, and M. N. Gurcan, "Computer-aided characterization of mammographic masses: Accuracy of mass segmentation and its effects on characterization," IEEE Trans. Med. Imaging **20**, 1275–1284 (2001).
[25]D. P. Huttenlocher, G. A. Klanderman, and W. J. Rucklidge, "Comparing images using the Hausdorff distance," IEEE Trans. Pattern Anal. Mach. Intell. **15**, 850–863 (1993).
[26]L. Hadjiiski, H. P. Chan, B. Sahiner, N. Petrick, and M. A. Helvie, "Automated registration of breast lesions in temporal pairs of mammograms for interval change analysis—Local affine transformation for improved localization," Med. Phys. **28**, 1070–1079 (2001).
[27]L. Hadjiiski, B. Sahiner, H. P. Chan, N. Petrick, M. A. Helvie, and M. N. Gurcan, "Analysis of temporal change of mammographic features: Computer-aided classification of malignant and benign breast masses," Med. Phys. **28**, 2309–2317 (2001).
[28]J. Wei, B. Sahiner, L. M. Hadjiiski, H.-P. Chan, M. A. Helvie, M. A. Roubidoux, C. Zhou, J. Ge, and Y. Zhang, "Two-view information fusion for improvement of computer-aided detection (CAD) of breast masses on mammograms," Proc. SPIE **6144**, 241–247 (2006).
[29]Y.-T. Wu, J. Wei, L. M. Hadjiiski, B. Sahiner, C. Zhou, J. Ge, J. Shi, Y. Zhang, and H. P. Chan, "Bilateral analysis based false positive reduction for computer-aided mass detection," Med. Phys. **34**, 3334–3344 (2007).
[30]B. Zheng, J. K. Leader, G. S. Abrams, A. H. Lu, L. P. Wallace, G. S. Maitz, and D. Gur, "Multiview-based computer-aided detection scheme for breast masses," Med. Phys. **33**, 3135–3143 (2006).
[31]H. P. Chan, B. Sahiner, R. F. Wagner, and N. Petrick, "Classifier design for computer-aided diagnosis: Effects of finite sample size on the mean performance of classical and neural network classifiers," Med. Phys. **26**, 2654–2668 (1999).
[32]B. Sahiner, H. P. Chan, and L. Hadjiiski, "Classifier performance prediction for computer-aided diagnosis using a limited data set," Med. Phys. **35**, 1559–1570 (2008).
[33]E. D. Pisano, C. Gatsonis, E. Hendrick, and M. Yaffe, "Diagnostic performance of digital versus film mammography for breast-cancer screening," N. Engl. J. Med. **353**, 1773–1783 (2005).